scientific reports

Check for updates

OPEN

Aggregation-induced emission from optically active X-shaped molecules based on planar chiral [2.2]paracyclophane

Keishi Jikuhara, Ryo Inoue & Yasuhiro Morisaki✉

An optically active π-stacked molecule was synthesized incorporating planar chiral [2.2] paracyclophane and *o*-carborane units to impart circularly polarized luminescence and aggregation-induced emission properties to the molecule. The molecule exhibited a strong emission from the aggregated state in a mixed solvent system (H_2O/THF) and the solid state in the PMMA matrix. In the aggregated state, weak circularly polarized luminescence was observed owing to the random intermolecular orientation. On the other hand, the circularly polarized luminescence was clearly observed in the PMMA film containing 1 wt% molecule. Theoretical studies using time-dependent density functional theory reproduced the molecule's circular dichroism and circularly polarized luminescence properties.

Aggregation-induced emission (AIE) is a well-known emission phenomenon[1–3], in which molecules are emissive upon aggregate formation and are not emissive in their solution states. Generally, fluorophores exhibit strong emission in the isolated states, such as in solution, and aggregation-caused quenching (ACQ) occurs in the aggregates, solids, and crystals. In 2001, Tang et al. reported that 1-methyl-1,2,3,4,5-pentaphenylsilole was effectively emissive in the aggregated state despite the absence of fluorescence in the diluted solution[4]. Therefore, researchers have prepared a wide variety of molecules exhibiting AIE using various AIE-active units, such as arylenevinylenes[5,6] in addition to the pentaphenyl siloles[4]. A typical AIE mechanism arises from the suppressing molecular motions in the aggregates. Interference of intermolecular interactions among π-conjugated fluorophores allows to generate bright AIE. In 2008, Chujo reported that *o*-carborane-based π-conjugated molecules exhibited the AIE properties[7]. When the stretching vibration of the carbon–carbon bond in the *o*-carborane unit[8] is frozen by aggregation, the non-radiative decay of the π-conjugated units is suppressed, leading to AIE from the aggregates and solids. This emission is a charge-transfer (CT) process between the electron-rich π-conjugated moieties substituted directly at the carbon of *o*-carborane and the electron-poor *o*-carborane unit. The significance of the dihedral angle between the carbon–carbon bond in the *o*-carborane unit and π-conjugated plane has also been reported[9,10].

[2.2]Paracyclophane is a cyclic compound in which two phenylene groups are stacked in close proximity[11–13]. Since its discovery[14] and practical synthesis[15], various [2.2]paracyclophane derivatives have been synthesized. The rotatory motion of the phenylenes in [2.2]paracyclophane is entirely suppressed because of the closely stacked phenylenes; therefore, [2.2]paracyclophanes with substituent(s) become planar chiral compounds depending on the substitution position(s)[16–27]. Planar chiral [2.2]paracyclophane derivatives have been utilized as chiral ligands and chiral auxiliaries in the fields of organometallic and organic chemistry. However, until recently, they were not employed in the fields of polymer and materials chemistry. In 2012, the synthesis of conjugated polymers bearing planar chiral pseudo-*ortho*-disubstituted [2.2]paracyclophane repeating units was reported[28]. The obtained optically active polymer emitted circularly polarized luminescence (CPL) with a relatively high anisotropy factor (g_{lum} value; $g_{lum} = 2(I_{left} - I_{right})/(I_{left} + I_{right})$, where I_{left} and I_{right} are photoluminescence intensities of the left-handed and right-handed CPL)[29–31] of the order of 10^{-3}. A variety of optically active conjugated molecules, such as polymers[28,32,33], macrocycles[34,35], and π-stacked dimers[36–39] comprising planar chiral [2.2] paracyclophanes, have been prepared, and their CPL behaviors have been investigated in detail. The researches on the CPL-emitters using chiral scaffolds including planar chiral [2.2]paracyclophanes have started a short time, and it is meaningful to prepare solid CPL emissive materials by combining AIEgens and chiral building

Department of Applied Chemistry for Environment, School of Biological and Environmental Sciences, Kwansei Gakuin University, 1 Gakuen Uegahara, Sanda, Hyogo 669-1330, Japan. ✉email: ymo@kwansei.ac.jp

blocks and to elucidate their emission behaviors for promising applications in three-dimensional display device, security ink, plant growth promoting film, biological imaging material, and so on[40–42]. In this study, *o*-carborane and planar chiral [2.2]paracyclophane were fused in a molecule, creating a conjugated molecule exhibiting aggregation-induced CPL. *o*-Carborane and planar chiral [2.2]paracyclophane units afforded AIE and CPL properties of the π-conjugated moiety, respectively. This research provides insights into the synthetic routes and optical properties of the novel molecule.

Results and discussions

Figure 1 illustrates the synthetic route for the (S_p)-isomer of the target molecule. Optically active bis-(*para*)-pseudo-*meta*-tetrasubstituted [2.2]paracyclophane (S_p)-**1** was prepared according to a previously reported method[43]. The bis-(*para*)-pseudo-*meta*-isomer was chosen instead of the corresponding pseudo-*ortho*-isomer attributed to the bulky *o*-carborane moieties located at pseudo-*meta*-positions. The chemoselective Sonogashira-Hagihara coupling[44,45] of (S_p)-**1** with trimethylsilylacetylene (TMS-acetylene) using a $Pd_2(dba)_3$/$^tBu_3P$/CuI catalytic system (dba = dibenzylideneacetone) afforded (S_p)-**2** in 77% isolated yield (Fig. 1A); in this reaction, bromo groups were reacted selectively. The remaining trifluoromethanesulfonyl (TfO) groups were reacted with triisopropylsilylacetylene (TIPS-acetylene) in the presence of a catalytic amount of $Pd_2(dba)_3$, 1,1'-bis(diphenylphosphino)ferrocene (dppf), and CuI to afford (S_p)-**3** in 88% isolated yield. The TMS groups were selectively removed by reacting (S_p)-**3** with K_2CO_3 and MeOH to yield (S_p)-**4** (77%). Sonogashira-Hagihara coupling of (S_p)-**4** with 4-dodecyloxy-1-iodobenzene **5** afforded (S_p)-**6** quantitatively. The dodecyloxy ($OC_{12}H_{25}$) group was incorporated to enhance the solubility and film-forming ability of the target molecule. The TIPS groups were removed by reacting (S_p)-**6** with Bu_4NF to afford (S_p)-**7** quantitatively (Fig. 1A). Finally, Sonogashira-Hagihara coupling of (S_p)-**7** with iodo-substituted *o*-carborane compound **10** (Fig. 1C), which was obtained in 68% isolated yield by the reaction of decaborane ($B_{10}H_{14}$) **8** with *p*-iodotolane **9** (Fig. 1B), afforded the target molecule (S_p)-**11** in 81% isolated yield. The (R_p)-isomer (R_p)-**11** was prepared following the same procedure as for (S_p)-**11** from enantiopure (R_p)-**1**. The structures of new compounds were confirmed by NMR spectroscopy and high-resonance mass (HRMS) spectrometry. Optical and chiroptical properties were investigated by specific rotation, ultraviolet–visible (UV–vis) absorption, PL, circular dichroism (CD) and CPL spectroscopy. Toxicity and/or biological activity of **11** for biological imaging applications were not investigated in the present stage.

Figure 2A shows the UV–vis absorption spectrum of (S_p)-**11** in tetrahydrofuran (THF) (1.0×10^{-5} M), revealing the π-π* absorption band of the phenylene-ethynylene moiety with molar absorption coefficient (ε) of 0.76×10^{-5} M^{-1} cm^{-1} at absorption maximum (λ_{max}) of 367 nm. The photoluminescence (PL) spectra of (S_p)-**11** in a mixed solution (1.0×10^{-5} M) of THF and H_2O are shown in Fig. 2B; THF and H_2O are good and poor solvents for (S_p)-**11**, respectively. Weak emission was observed in 100% THF solution, whereas a strong emission peak was observed (peak top λ_{max} = 609 nm) in the THF/H_2O mixed solution (H_2O 90 volume% = vol%) with a PL quantum yield (Φ_{PL}) of 13%. Figure 2C shows their PL excited at 365 nm using a handy UV lamp. Figure 2D shows the UV–vis absorption spectra of (S_p)-**11** in a mixed solution (1.0×10^{-5} M) of THF and H_2O. The spectra were gradually red-shifted with increasing H_2O volume. A broad band appeared as a tailing peak in the longer-wavelength region, when the H_2O content was greater than 50 vol%, suggesting the formation of aggregates of (S_p)-**11**. In Fig. 2E, the PL intensities are plotted against H_2O vol%, indicating that the AIE of (S_p)-**11** was correspondingly observed over 50 vol% of H_2O.

Weak emission was detected around 445 nm, as shown in the inset of Fig. 2B, which can be observed in a series of X-shaped molecules[32,37,46,47]. These PL signals were not affected by the polarity change arose from the formation of aggregates; therefore, they were assigned to the general PL peaks of the X-shaped skeleton[32,37,46,47]. On the other hand, a clear blue-shift was observed for the strong emission peaks; for example, emission peak top in the THF/H_2O (10/90) solution appeared at 609 nm, and that appeared at 771 nm in the THF/H_2O (90/10) solution. It is suggested that the main emission of the carborane-containing π-conjugated molecules is caused by the intramolecular charge-transfer (vide infra) in the S_1 state[7,9,10]. The aggregates are formed by hydrophobic effect in the H_2O-concentrated solutions, and the inside of the aggregates becomes a low polar environment, leading to the blue-shift of the intramolecular CT emission peaks and the increase of the emission intensities owing to the immobility of the molecule[48,49].

Figure 3 shows the UV–vis absorption and PL spectra of the neat film of (S_p)-**11** fabricated using the drop-casting method from the toluene solution containing 1 wt% of (S_p)-**11** and a poly(methyl methacrylate) (PMMA) film containing 1 wt% of (S_p)-**11**. The UV–vis absorption spectrum of the neat film reached a ceiling, exhibiting a red-shift attributed to the intermolecular interactions. The PL spectra of the neat film were also red-shifted compared to those of the (S_p)-**11**-dispersed PMMA film. The calculated Φ_{PL}s of the neat and PMMA films were 21% and 58%, respectively. In the PMMA film, (S_p)-**11** was dispersed and isolated, resulting in a bright yellow AIE.

The CD and CPL properties of the aggregates of **11** in THF and H_2O (H_2O 90 vol%) and **11**-dispersed PMMA film and were investigated; their spectra are shown in Fig. 4. As shown in Fig. 4A, the mirror image CD spectra were observed for both the enantiomers of aggregates **11**, with the first Cotton effects of the (S_p)- and (R_p)-isomers being positive and negative, respectively. These signs are identical to those of a series of optically active X-shaped molecules reported previously[32,36,37,46]. However, their noisy CPL signals were barely detected (Fig. 4B), its absolute anisotropy factor ($|g_{lum}|$ value) was estimated to be 0.2×10^{-3} at the highest. The signs were the same as those of the first Cotton effects. In the aggregates, the molecules were π-stacked intermolecularly without ordered structures, namely, random higher-ordered structures, resulting in weak and noisy CPL spectra.

Figure 4C shows the CD spectra of the PMMA films including **11**, and the mirror image spectra were observed. The spectra and signs were similar to those of the aggregates (Fig. 4A). As shown in Fig. 4D, the CPL was clearly observed, and the signs were also identical to those of the first Cotton effects. The $|g_{lum}|$ value of the PMMA films containing **11** was calculated to be 0.6×10^{-3}.

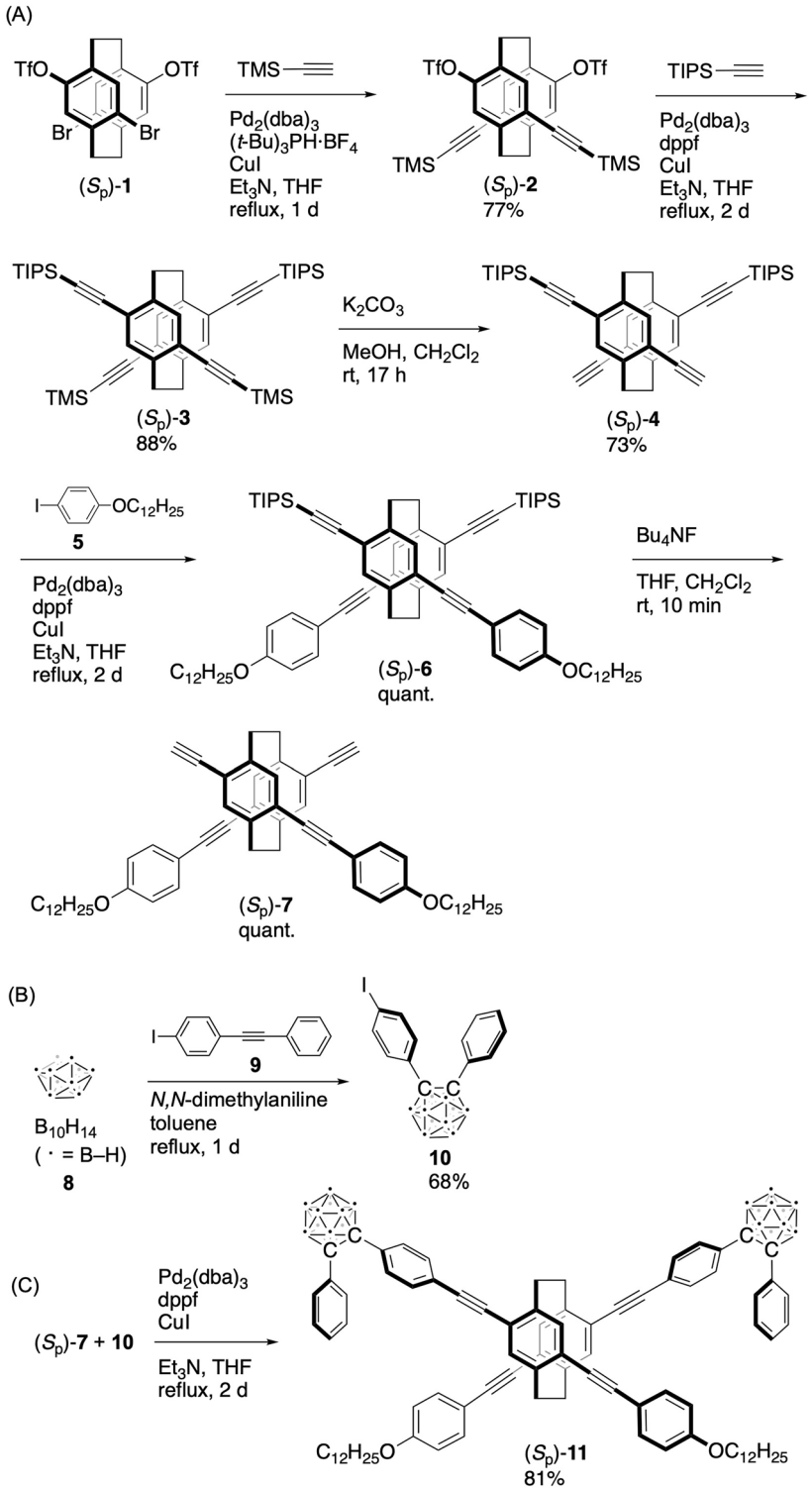

Figure 1. Synthesis of the optically active X-shaped molecule consisting of planar chiral [2.2]paracyclophane and *o*-carboranes.

The molecular orbitals of the model compound, in which the dodecyloxy groups of (S_p)-**11** were replaced with methoxy groups, in the ground state were calculated using density functional theory (DFT) and compared with those of the X-shaped molecule prepared recently[46], as shown in Fig. 5. Both molecules exhibited delocalized orbitals (highest occupied molecular orbital (HOMO), HOMO−1, lowest unoccupied molecular orbital (LUMO), and LUMO + 1) extending over the entire molecule via through-space interactions between the central benzene rings. The LUMO and LUMO + 1 in the (S_p)-**11** model were primarily located on the benzene rings with

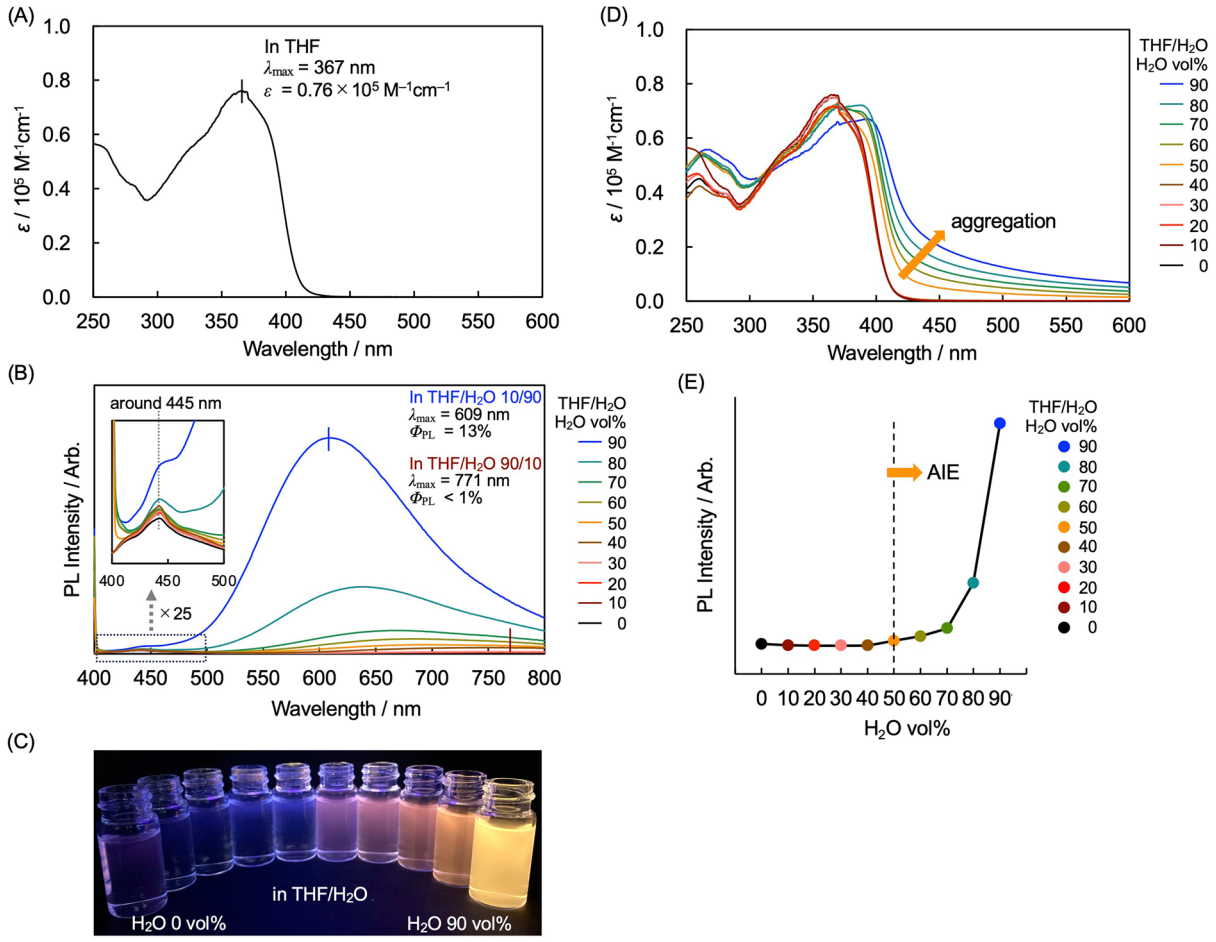

Figure 2. (**A**) UV–vis absorption spectrum of (S_p)-**11** in THF (1.0×10^{-5} M). (**B**) PL spectra of (S_p)-**11** in THF/H_2O (1.0×10^{-5} M) excited at each absorption maximum. Inset: expanded view of the vertical axis from 400 to 500 nm. (**C**) PL in THF/H_2O (1.0×10^{-5} M) excited using a handy UV lamp ($\lambda = 365$ nm). (**D**) UV–vis absorption spectra of (S_p)-**11** in THF/H_2O (1.0×10^{-5} M). (**E**) Dependence of PL intensity at λ_{max} of each emission peak on the solvent composition (H_2O vol% of THF/H_2O).

carborane units, and the HOMO and HOMO–1 were primarily located on the methoxybenzene rings owing to the electron-withdrawing character of the carborane moiety. The carborane units decreased all the energy levels in the (S_p)-**11** model, resulting in lower energy levels than those in the corresponding X-shaped molecule. The simulated CD spectrum of the (S_p)-**11** model and parameters related to the transitions, which was simulated using time-dependent DFT (TD-DFT) calculations, are shown in Supplementary Fig. 30 and Supplementary Table 1 in the Supporting Information (SI). Transition from the HOMO to LUMO was allowed according to the oscillator strength, and the strong rotatory strength was estimated (Supplementary Table 1). The sign of the first Cotton effect observed in the (S_p)-**11** model was positive, supporting the experimental results for (S_p)-**11** (Fig. 4C).

Figure 6A shows the LUMOs and HOMOs in the S_1 states of the (S_p)-**11** model, and Fig. 6B shows those of the corresponding X-shaped molecule[46]. Their orbitals were similar; the LUMOs were delocalized throughout the molecules, and the HOMOs were localized on one of the two π-electron systems. Figure 6B presents a side view of the LUMO in the S_1 state of the (S_p)-**11** model. The antibonding orbital of the C–C bond in the carborane unit was overlapped with a portion of the antibonding orbitals of the benzene ring to form σ*-π* conjugation[7,9,10]. The LUMO and HOMO in the in the S_1 states of the (S_p)-**11** model were slightly biased toward the carborane and methoxybenzene moieties, respectively, highlighting the CT emission of (S_p)-**11**.

Figure 7 shows the simulation results for the electric and magnetic transition dipole moments ($\boldsymbol{\mu}$ and $\boldsymbol{m}$, respectively) in the S_1 states of the (S_p)-**11** model and the corresponding X-shaped molecule[46]. The CPL $g_{lum,calcd}$ value can be calculated using the following equation: $g_{lum,calcd} = 4|\boldsymbol{\mu}||\boldsymbol{m}|\cos\theta_{\mu,m}/(|\boldsymbol{\mu}|^2+|\boldsymbol{m}|^2)$, where $\theta_{\mu,m}$ is the angle between $\boldsymbol{\mu}$ and $\boldsymbol{m}$[29–31]. The $\boldsymbol{\mu}$s in both molecules were extended along the long axis of one of the π-electron systems. The $\theta_{\mu,m}$ of the (S_p)-**11** model was closer to 90° than that of the corresponding X-shaped molecule, and the smaller $g_{lum,calcd}$ value of $+0.4 \times 10^{-3}$ was obtained. The observed $g_{lum,obsd}$ values of (S_p)-**11** and the X-shaped molecule were found to be $+0.6 \times 10^{-3}$ and $+1.1 \times 10^{-3}$, respectively. The sign and the order of the magnitude of the $g_{lum,calcd}$ values were consistent with those of the observed $g_{lum,obsd}$ values.

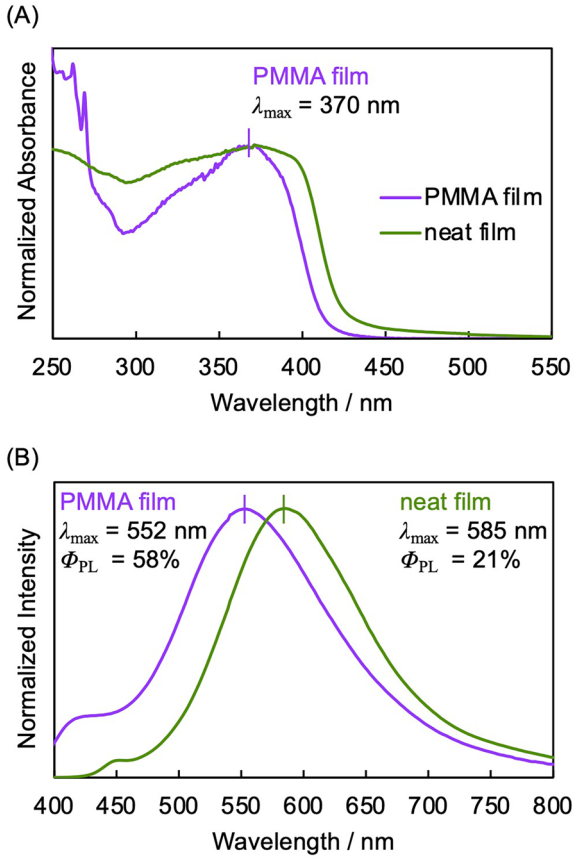

Figure 3. (**A**) UV–vis absorption spectra of the neat film of (S_p)-**11** and the PMMA film containing 1 wt% of (S_p)-**11**. (**B**) PL spectra of the neat film of (S_p)-**11** and the PMMA film containing 1 wt% of (S_p)-**11**, excited at 370 nm. The neat film was fabricated on a quartz plate by a drop-casting method using toluene solution; 0.5 mg of (S_p)-**11** in toluene 5.0 mL. The PMMA film was fabricated on a quartz plate by a drop-casting method using toluene solution; 0.5 mg of (S_p)-**11** and 49.5 mg of PMMA in toluene 5.0 mL. The obtained films were air-dried, and then, vacuum-dried.

Conclusion

Optically active π-stacked molecules comprising planar chiral [2.2]paracyclophane and *o*-carboranes were synthesized from enantiopure bis-(*para*)-pseudo-*meta*-tetrasubstituted [2.2]paracyclophanes. An X-shaped structure was constructed using the [2.2]paracyclophane unit, with *o*-carboranes located at the pseudo-*meta*-positions. Although the molecule did not exhibit emission in solution, it displayed emission in the form of aggregates (i.e. suspensions and films), exhibiting AIE properties. In particular, efficient emission was observed for molecules dispersed in the PMMA film. The PMMA film containing the molecule exhibited CPL properties with a moderate anisotropy factor of 0.6×10^{-3}. This emission was derived from the CT emission from the carborane-containing benzene unit to the methoxybenzene unit. The CD and CPL behaviors were well-reproduced by simulations using TD-DFT calculations.

Experimental section

General

^{1}H (500 MHz), ^{13}C (125 MHz), and ^{11}B (160 MHz) NMR spectra were recorded on a JEOL JNM ECZ-500R instrument. Samples were analyzed in $CDCl_3$, and the chemical shift values were expressed relative to Me_4Si for ^{1}H and ^{13}C NMR spectra and $BF_3{\cdot}H_2O$ spectra for ^{11}B NMR for as internal standards. Analytical thin layer chromatography (TLC) was performed with silica gel 60 Merck F_{254} plates. Column chromatography was performed with Wakogel C-300 SiO_2. Recyclable high-performance liquid chromatography (HPLC) was carried out on a YMC LC Forte/R. High-resolution mass (HRMS) spectra were obtained on a Bruker Daltonics microTOF II spectrometer (ESI and APCI) using sodium formate and tuning mix as internal standards. UV–vis spectra were recorded on a JASCO V-730 spectrophotometer, and samples were analyzed at room temperature. PL spectra were recorded on a JASCO FP-8500 spectrofluorometer, and samples were analyzed at room temperature. Absolute PL quantum efficiency was calculated on a JASCO FP8500 with an ILF-835 integrating sphere. Specific rotations ($[\alpha]^{t}_{D}$) were measured with a HORIBA SEPA-500 polarimeter. CD spectra were recorded on a JASCO J-1500 spectropolarimeter with THF as a solvent at room temperature. CPL spectra were recorded on a JASCO CPL-300 with THF as a solvent at room temperature.

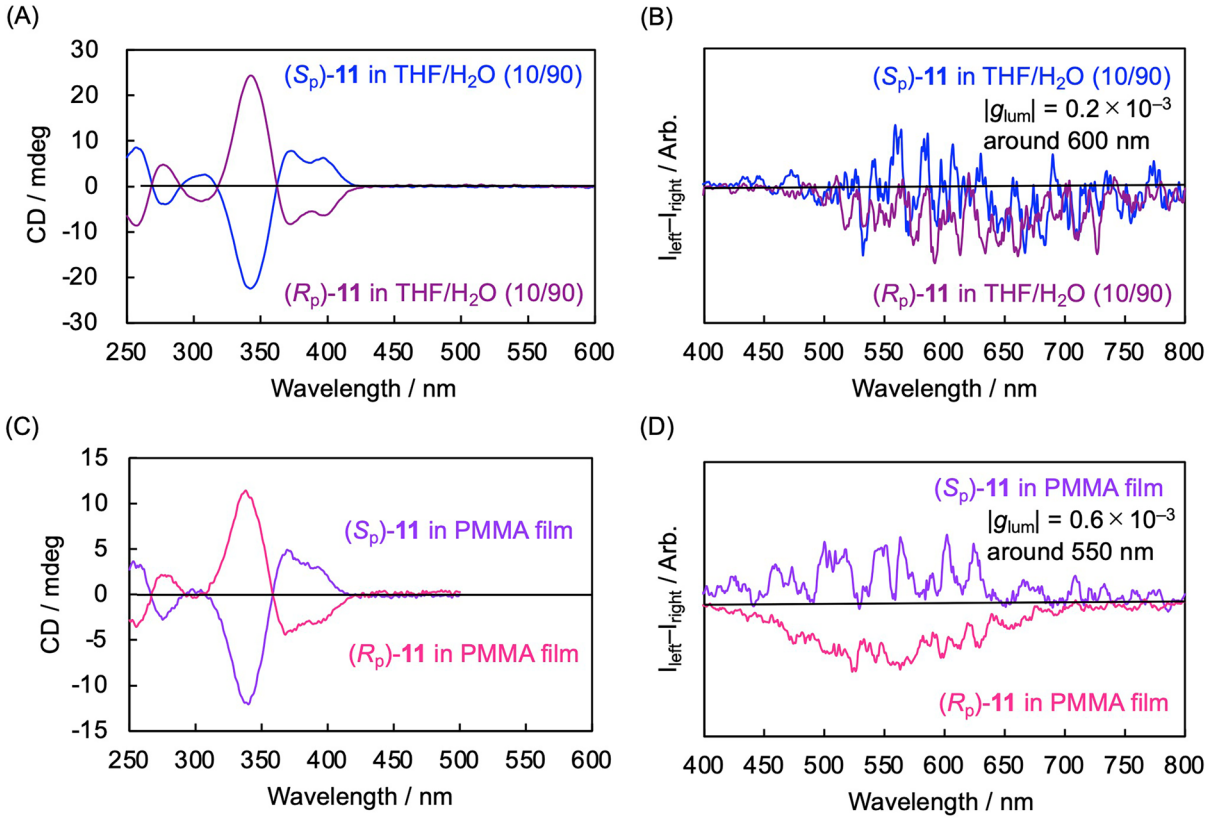

Figure 4. (**A**) CD spectra of (S_p)-**11** in THF/H_2O (10/90 vol/vol, 1.0×10^{-5} M). (**B**) CPL spectra of (S_p)-**11** in THF/H_2O (10/90 vol/vol, 1.0×10^{5} M), excited at 300 nm. (**C**) CD spectra of the PMMA film containing 1 wt% of (S_p)-**11**. (**D**) CPL spectra of the PMMA film containing 1 wt% of (S_p)-**11**, excited at 300 nm.

Materials

Commercially available compounds used without purification are as follows: trimethylsilylacetylene, triisopropylsilylacetylene, decaborane ($B_{10}H_{14}$), *N*,*N*-dimethylaniline, *N*,*N*-dimethylformamide (DMF), Bu_4NF (1.0 M THF), $Pd_2(dba)_3$, (*t*-Bu)$_3$P·HBF_4, dppf, CuI, KOH, K_2CO_3, KI, CH_2Cl_2, MeOH, THF (dehaydrated), toluene (dehaydrated), pyridine. Et_3N was purchased and purified by distillation using KOH.

Compounds (S_p)-**1**[43], (R_p)-**1**[43], **5**[50] and **9**[51] were prepared according to the literature's procedures.

Synthesis of (S_p)-2

A mixture of (S_p)-**1** (660.2 mg, 0.99 mmol), $Pd_2(dba)_3$ (91.3 mg, 0.099 mmol), (*t*-Bu_3)P·HBF_4 (109.9 mg, 0.38 mmol), CuI (18.9 mg, 0.099 mmol), THF (10 mL), and Et_3N (10 mL) was placed in a round-bottom flask equipped with magnetic stirring bar. After degassing the reaction mixture several times, trimethylsilylacetylene (1.44 mL, 11 mmol) was added to the mixture via a syringe. The reaction was carried out at reflux temperature for 1 day with stirring. After the reaction mixture was cooled to room temperature, precipitates were removed by filtration, and the solvent was removed with a rotary evaporator. The residue was purified by column chromatography on SiO_2 ($CHCl_3$/hexane = 1/5 v/v as an eluent) to afford (S_p)-**2** (536.7 mg, 0.77 mmol, 77%) as a light yellow solid.

R_f = 0.35 ($CHCl_3$/hexane = 1/5 v/v). ^{1}H NMR ($CDCl_3$, 500 MHz): δ 0.31 (s, 18H), 2.84–3.01 (m, 4H), 3.27–3.48 (m, 4H), 6.77 (s, 2H), 6.99 (s, 2H) ppm; ^{13}C NMR ($CDCl_3$, 125 MHz) δ = 29.9, 32.0, 101.1, 102.5, 118.8 (q, J_{C-F} = 325 Hz), 125.1, 126.2, 132.1, 137.0, 145.7, 148.0 ppm. HRMS (ESI +): m/z calcd. for $C_{28}H_{30}F_6O_6S_2Si_2$ $[M + Na]^+$: 719.0819; found: 719.0834. $[\alpha]^{25}_D$ = + 39.46 (*c* 0.2, $CHCl_3$).

The enantiomer (R_p)-**2** was obtained in 90% yield by the same procedure. HRMS (ESI+): m/z calcd. for $C_{28}H_{30}F_6O_6S_2Si_2$ $[M + Na]^+$: 719.0819; found: 719.0800. $[\alpha]^{25}_D$ = − 39.44 (*c* 0.2, $CHCl_3$).

Synthesis of (S_p)-3

A mixture of (S_p)-**2** (125.5 mg, 0.17 mmol), $Pd_2(dba)_3$ (16.09 mg, 0.017 mmol), dppf (9.75 mg, 0.017 mmol), CuI (3.34 mg, 0.017 mmol), THF (15 mL), and Et_3N (15 mL) was placed in a round-bottom flask equipped with magnetic stirring bar. After degassing the reaction mixture several times, triisopropylsilylacetylene (0.52 mL, 1.7 mmol) was added to the mixture via a syringe. The reaction was carried out at reflux temperature for 2 days with stirring. After the reaction mixture was cooled to room temperature, precipitates were removed by filtration, and the solvent was removed with a rotary evaporator. The residue was purified by column chromatography on SiO_2 ($CHCl_3$/hexane = 1/9 v/v as an eluent) and by recyclable HPLC (CH_2Cl_2 as an eluent) to afford (S_p)-**3** (118.7 mg, 0.15 mmol, 88%) as a light yellow oil.

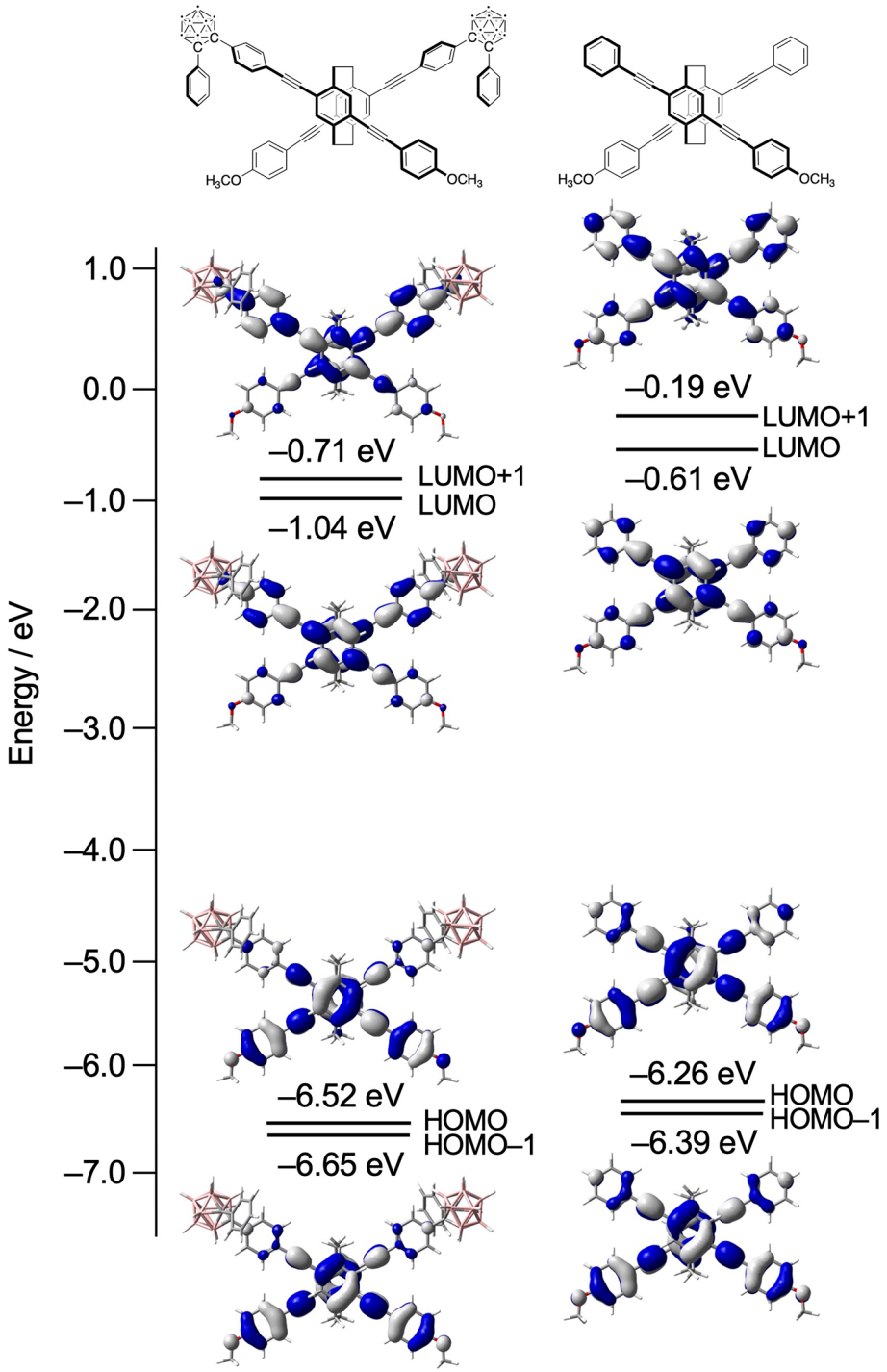

Figure 5. Molecular orbitals of the (S_p)-**11** model and the corresponding X-shaped molecule in the ground states determined with TD-DFT calculations (TD-CAM-B3LYP/6-31G(d)).

R_f = 0.78 ($CHCl_3$/hexane = 1/9 v/v). ^{1}H NMR ($CDCl_3$, 500 MHz): δ 0.29 (s, 18H), 1.19 (s, 42H), 2.90–2.99 (m, 4H), 3.37–3.45 (m, 4H), 6.98 (s, 2H), 7.01 (s, 2H) ppm; ^{13}C NMR ($CDCl_3$, 125 MHz) δ = 11.4, 18.6, 32.1, 95.5, 99.4, 104.5, 106.2, 124.9, 125.2, 134.2, 134.4, 142.1, 142.4 ppm. HRMS (ESI+): m/z calcd. for $C_{48}H_{72}Si_4$ $[M+Na]^+$: 786.4603; found: 786.4608. $[\alpha]^{25}_D$ = + 42.49 (*c* 0.1, $CHCl_3$).

The enantiomer (R_p)-**3** was obtained in 89% yield by the same procedure. HRMS (ESI): m/z calcd. for $C_{48}H_{72}Si_4$ $[M+Na]^+$: 786.4603; found: 786.4604. $[\alpha]^{25}_D$ = − 42.66 (*c* 0.1, $CHCl_3$).

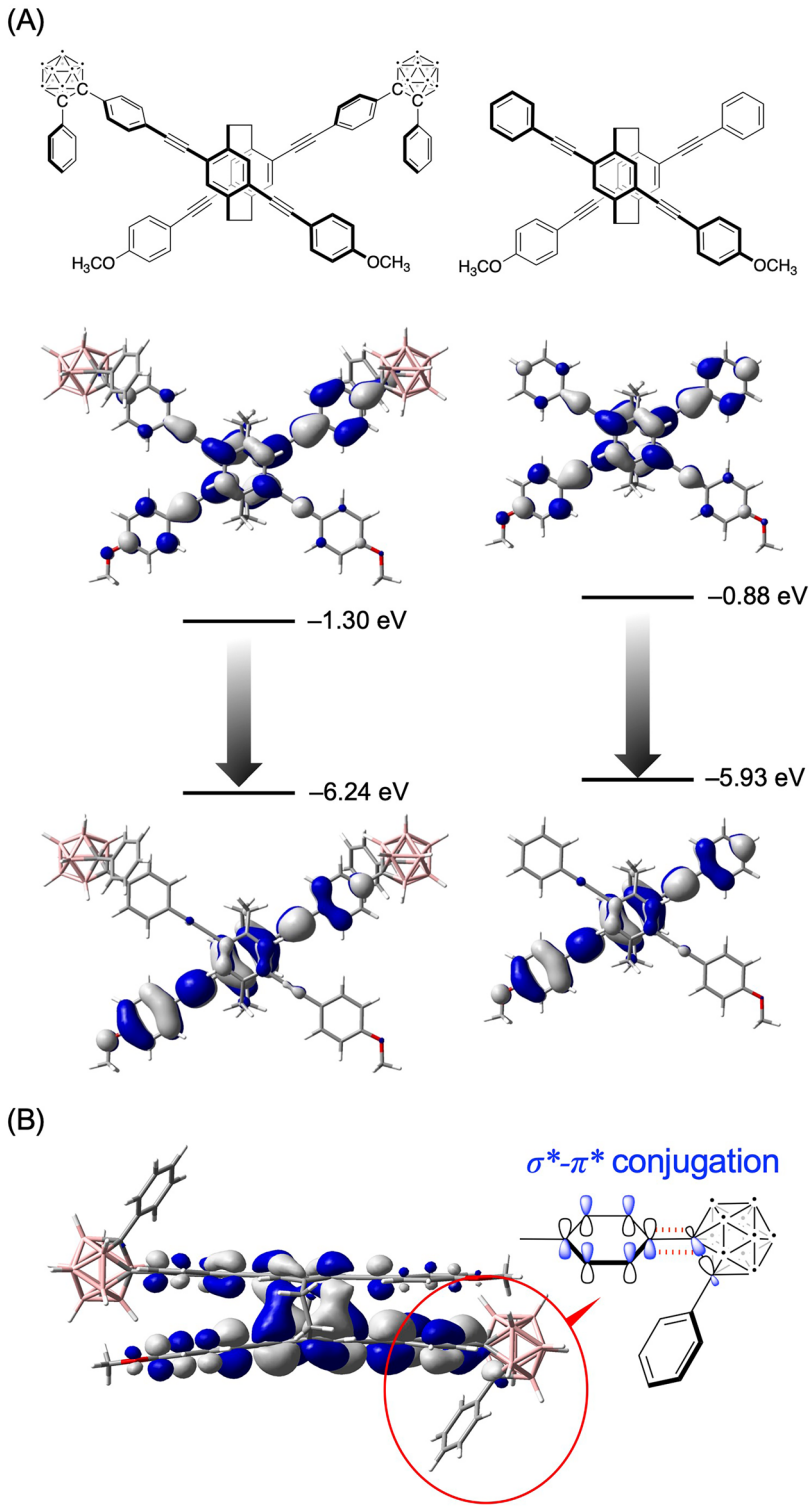

Figure 6. (**A**) Molecular orbitals of the (S_p)-**11** model and the corresponding X-shaped molecule in the S_1 states determined with TD-DFT calculations (TD-CAM-B3LYP/6-31G(d)). (**B**) Side view of the HOMO of the (S_p)-**11** model in the S_1 state, showing σ*-π* conjugation.

Synthesis of (S_p)-4

K_2CO_3 (142.5 mg, 1.03 mmol) was added to a suspension of (S_p)-**3** (196.3 mg, 0.25 mmol) in MeOH (80 mL) and CH_2Cl_2 (10 mL). After the mixture was stirred for 17 h at room temperature, H_2O was added to the reaction

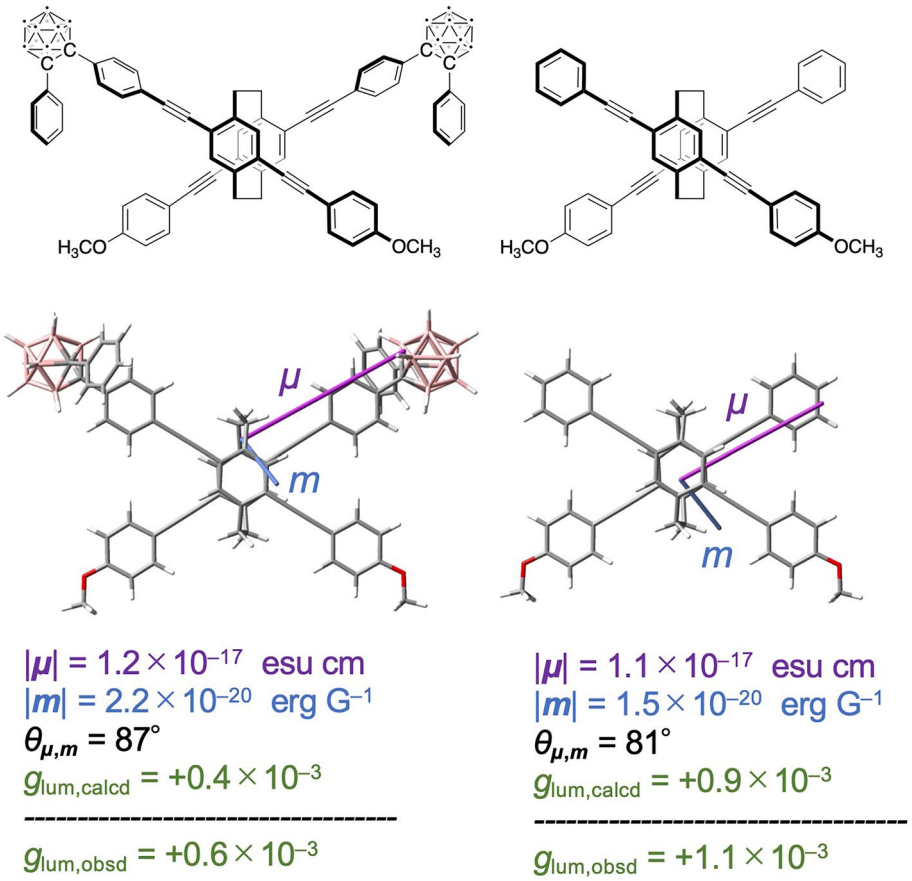

Figure 7. Simulation results for the transition dipole moments ($\boldsymbol{\mu}$ = electric transition dipole moment and $\boldsymbol{m}$ = magnetic transition dipole moment) of the (S_p)-**11** model and the corresponding X-shaped molecule in the S_1 state (TD-CAM-B3LYP/6-31G(d)//CAM-B3LYP/6-31G(d)).

mixture. The organic layer was extracted with $CHCl_3$ and washed with brine. The combined organic layer was dried over $MgSO_4$. $MgSO_4$ was removed by filtration, and the solvent was removed with a rotary evaporator. The residue was purified by column chromatography on SiO_2 ($CHCl_3$/hexane = 1/9 v/v as an eluent) to afford (S_p)-**4** (116.8 mg, 0.18 mmol, 73%) as colorless needles.

R_f = 0.69 ($CHCl_3$/hexane = 1/9 v/v). ^{1}H NMR ($CDCl_3$, 500 MHz): δ 1.19 (s, 42H), 2.94–3.01 (m, 4H), 3.31 (s, 2H), 3.38–3.47 (m, 4H), 7.03 (s, 2H), 7.09 (s, 2H) ppm; ^{13}C NMR ($CDCl_3$, 125 MHz) δ = 11.4, 18.7, 18.8, 31.9, 32.1, 81.8, 82.8, 95.9, 106.0, 123.9, 125.8 134.7 134.9, 142.0, 142.3 ppm. HRMS (ESI): m/z calcd. for $C_{42}H_{56}Si_2$ $[M + Na]^+$: 639.3813; found: 639.3805. $[\alpha]^{25}_D$ = + 52.57 (*c* 0.2, $CHCl_3$).

The enantiomer (R_p)-**4** was obtained in 75% yield by the same procedure. HRMS (ESI): m/z calcd. for $C_{42}H_{56}Si_2$ $[M + Na]^+$: 639.3813; found: 639.3785. $[\alpha]^{25}_D$ = − 52.28 (*c* 0.2, $CHCl_3$).

Synthesis of (S_p)-6

A mixture of (S_p)-**4** (32.0 mg, 0.051 mmol), **5** (44.26 mg, 0.11 mmol), $Pd_2(dba)_3$ (4.74 mg, 0.0051 mmol), dppf (2.87 mg, 0.0051 mmol), CuI (0.98 mg, 0.0051 mmol), THF (10 mL), and Et_3N (10 mL) was placed in a round-bottom flask equipped with magnetic stirring bar. The reaction was carried out at reflux temperature for 2 days with stirring. After the reaction mixture was cooled to room temperature, precipitates were removed by filtration, and the solvent was removed with a rotary evaporator. The residue was purified by column chromatography on SiO_2 ($CHCl_3$/hexane = 1/9 v/v as an eluent) and by recyclable HPLC (CH_2Cl_2 as an eluent) to afford (S_p)-**6** (36.5 mg, 0.032 mmol, quant.) as a light yellow oil.

R_f = 0.20 ($CHCl_3$/hexane = 1/9 v/v). ^{1}H NMR ($CDCl_3$, 500 MHz): δ 0.88 (t, *J* = 7.0 Hz, 6H), 1.19 (s, 42H), 1.27–1.50 (36H), 1.80 (m, 4H), 3.00–3.04 (m, 4H), 3.44–3.53 (m, 4H), 3.99 (t, *J* = 6.5 Hz, 4H), 6.89 (d, *J* = 8.6 Hz, 4H), 7.07 (s, 2H), 7.09 (s, 2H), 7.48 (d, *J* = 8.0 Hz, 4H); ^{13}C NMR ($CDCl_3$, 125 MHz) δ = 11.5, 14.1, 18.8, 22.7, 26.0, 29.2, 29.4, 29.6, 31.9, 68.1, 87.7, 94.7, 95.2, 106.6, 114.4, 114.6, 115.4, 124.7, 125.5, 132.9, 130.0, 133.8, 134.0, 134.9, 135.1, 141.6, 142.2, 159.2 ppm. HRMS (ESI): m/z calcd. for $C_{78}H_{112}O_2Si_2$ $[M + Na]^+$: 1159.8093; found: 1159.8078. $[\alpha]^{25}_D$ = + 331.18 (*c* 0.1, $CHCl_3$).

The enantiomer (R_p)-**6** was obtained in 88% yield by the same procedure. HRMS (ESI): m/z calcd. for $C_{78}H_{112}O_2Si_2$ $[M + Na]^+$: 1159.8093; found: 1159.8136. $[\alpha]^{25}_D$ = − 331.23 (*c* 0.1, $CHCl_3$).

Synthesis of (S_p)-7

(S_p)-**6** (87.0 mg, 0.076 mmol) was dissolved in THF (15 mL), followed by the addition of Bu_4NF (1.0 M THF solution, 1.0 mL) via a syringe. The reaction was carried out at room temperature for 10 min, H_2O was added to the reaction mixture. The organic layer was extracted three times with $CHCl_3$ and washed with brine, and dried over $MgSO_4$. $MgSO_4$ was removed by filtration, and the solvent was removed by a rotary evaporator. The residue was purified by column chromatography on SiO_2 ($CHCl_3$/hexane = 2/3 v/v as an eluent) and by recyclable HPLC (CH_2Cl_2 as an eluent) to afford (S_p)-**7** (40.0 mg, 0.048 mmol, quant.) as a light yellow oil.

R_f = 0.55 ($CHCl_3$/hexane = 2/3 v/v). ^{1}H NMR ($CDCl_3$, 500 MHz): δ 0.88 (t, J = 7.0 Hz, 6H), 1.27–1.49 (36H), 1.80 (m, 4H), 3.00–3.05 (m, 4H), 3.37 (s, 2H), 3.43–3.50 (m, 4H), 3.99 (t, J = 7.0 Hz, 4H), 6.90 (d, J = 8.6 Hz, 4H), 7.03 (s, 2H), 7.11 (s, 2H), 7.50 (d, J = 8.6 Hz, 4H) ppm; ^{13}C NMR ($CDCl_3$, 125 MHz) δ = 14.1, 22.7, 26.0, 29.1, 29.3, 29.5, 29.6, 31.9, 32.0, 32.5, 68.1, 81.5, 83.1, 87.4, 94.8, 114.6, 115.3, 123.2, 126.1, 132.9, 134.1, 134.9, 141.6, 142.5, 159.3 ppm. HRMS (ESI): m/z calcd. for $C_{60}H_{72}O_2$ $[M+Na]^+$: 847.5425; found: 847.5389. $[\alpha]^{25}_D$ = + 55.51 (c 0.1, $CHCl_3$).

The enantiomer (R_p)-**7** was obtained quantitatively by the same procedure. HRMS (ESI): m/z calcd. for $C_{60}H_{72}O_2$ $[M+Na]^+$: 847.5425; found: 847.5416. $[\alpha]^{25}_D$ = − 55.29 (c 0.05, $CHCl_3$).

Synthesis of 10

The mixture of compound **9** (914.2 mg, 3.01 mmol) and decaborane **8** (423.5 mg, 3.46 mmol) was dissolved in dry toluene (15 mL) at room temperature. *N*,*N*-Dimethylaniline (0.64 mL, 5.04 mmol) was added, and the mixture was refluxed for 24 h. After cooling to room temperature, solvent was separated from the solid and evaporated. The residue was purified by column chromatography on SiO_2 (hexane as an eluent). Recrystallization from $CHCl_3$ and MeOH to provide compound **10** (862.9 mg, 2.03 mmol, 68%) as a colorless crystal.

R_f = 0.28 (hexane). ^{1}H NMR ($CDCl_3$, 500 MHz): δ 1.90–3.71 (br, 10H), 7.11 (d, J = 8.6 Hz, 2H), 7.16 (t, J = 8.0, 2H), 7.27 (d, J = 7.0 Hz, 1H), 7.41 (d, J = 7.5 Hz, 2H), 7.46 (d, J = 8.6 Hz, 2H); ^{13}C NMR ($CDCl_3$, 125 MHz) δ = 84.1, 85.1, 97.1 128.4, 130.3, 130.4, 130.5, 132.0. 137.4 ppm; ^{11}B NMR ($CDCl_3$, 160 MHz) δ = 3.56, 2.62, − 3.20, − 4.33 , − 5.36, − 6.61 ppm. HRMS (ESI): m/z calcd. for $C_{14}H_{19}B_{10}I$ $[M+Cl]^-$: 459.1161; found: 459.1159.

Synthesis of (S_p)-11

A mixture of (S_p)-**7** (40.0 mg, 0.048 mmol), **10** (49.23 mg, 0.116 mmol), $Pd_2(dba)_3$ (4.43 mg, 0.0048 mmol), dppf (5.37 mg, 0.0096 mmol), CuI (1.84 mg, 0.0096 mmol), THF (7.5 mL), and Et_3N (7.5 mL) was placed in a round-bottom flask equipped with magnetic stirring bar. The reaction was carried out at reflux temperature for 2 days with stirring. After the reaction mixture was cooled to room temperature, precipitates were removed by filtration, and the solvent was removed with a rotary evaporator. The residue was purified by column chromatography on SiO_2 ($CHCl_3$/hexane = 1/4 v/v as an eluent) and by recyclable HPLC (CH_2Cl_2 as an eluent) to afford (S_p)-**11** (27.9 mg, 0.019 mmol, 81%) as a yellow solid.

R_f = 0.28 ($CHCl_3$/hexane = 1/4 v/v). ^{1}H NMR ($CDCl_3$, 500 MHz): δ 0.88 (t, J = 6.5 Hz, 6H), 1.27–1.49 (36H), 1.83 (m, 4H), 1.90–2.88 (br, 20H), 2.92–3.06 (m, 4H), 3.38–3.50 (m, 4H), 4.02 (t, J = 6.5 Hz, 4H), 6.90 (d, J = 8.0 Hz, 4H), 6.95 (s, 2H), 7.08 (s, 2H), 7.17 (t, J = 8.0, 4H), 7.27–7.31 (m, 6H), 7.42–7.47 (m, 12H); ^{13}C NMR ($CDCl_3$, 125 MHz) δ = 14.1, 22.7, 26.0, 29.2, 29.3, 29.4, 29.6, 31.9, 32.5, 68.2, 84.5, 85.4, 87.6, 91.8, 92.7, 95.2, 114.6, 115.2, 123.8, 125.6, 126.1, 128.4, 130.3, 130.5, 130.6, 131.1, 132.9, 134.4, 134.6, 141.7, 159.4 ppm; ^{11}B NMR ($CDCl_3$, 160 MHz) δ = 2.7, −5.0 ppm. HRMS (ESI): m/z calcd. for $C_{88}H_{108}B_{20}O_2$ $[M+H]^+$: 1418.0422; found: 1418.0374. $[\alpha]^{25}_D$ = + 250.48 (c 0.1, $CHCl_3$).

The enantiomer (R_p)-**11** was obtained in 92% yield by the same procedure. HRMS (ESI): m/z calcd. for $C_{88}H_{108}B_{20}O_2$ $[M+H]^+$: 1418.0422; found: 1418.0386. $[\alpha]^{25}_D$ = − 250.22 (c 0.1, $CHCl_3$).

Data availability

The datasets used and/or analyzed during the current study available from the corresponding author on reasonable request.

Received: 9 August 2023; Accepted: 4 December 2023
Published online: 19 December 2023

References

1. Hong, Y., Lam, J. W. Y. & Tang, B. Z. Aggregation-induced emission: Phenomenon, mechanism and applications. *Chem. Commun.* **29**, 4332–4353 (2009).
2. Tang, B. Z. & Qin, A. *Aggregation-Induced Emission: Applications* (Wiley, 2013).
3. Tang, B. Z. & Qin, A. *Aggregation-Induced Emission: Fundamentals* (Wiley, 2013).
4. Kwok, H. S., Zhan, X., Liu, Y., Zhuc, D. & Tang, B. Z. Jingdong Luo, Zhiliang Xie, Jacky WY Lam, Lin Cheng, Haiying Chen, b Chengfeng Qiu, b. *Chem. Commun.* **1740**, 1741 (2001).
5. An, B.-K., Kwon, S.-K., Jung, S.-D. & Park, S. Y. Enhanced emission and its switching in fluorescent organic nanoparticles. *J. Am. Chem. Soc.* **124**, 14410–14415 (2002).
6. Zhao, Z., Lam, J. W. Y. & Tang, B. Z. Tetraphenylethene: A versatile AIE building block for the construction of efficient luminescent materials for organic light-emitting diodes. *J. Mater. Chem.* **22**, 23726–23740 (2012).
7. Kokado, K. & Chujo, Y. Emission via aggregation of alternating polymers with *o*-carborane and *p*-phenylene–ethynylene sequences. *Macromolecules* **42**, 1418–1420 (2009).
8. Carboranes, I. 1,2–$C_2B_{10}H_{12}$. In *Carboranes* 3rd edn (ed. Russell, N. G.) 283–502 (United Kingdom, 2016).
9. Naito, H., Morisai, Y. & Chujo, Y. *o*-carborane-based anthracene: A Variety of emission behaviors. *Angew. Chem. Int. Ed.* **54**, 5084–5087 (2015).
10. Naito, H., Nishino, K., Morisai, Y., Tanaka, K. & Chujo, Y. Highly-efficient solid-state emissions of anthracene-*o*-carborane dyads with various substituents and their thermochromic luminescence properties. *J. Mater. Chem. C* **5**, 10047–10054 (2017).

11. Vögtle, F. *Cyclophane Chemistry: Synthesis, Structures and Reactions* (John Wiley & Sons, 1993).
12. Gleiter, R. & Hopf, H. *Modern Cyclophane Chemistry* (Wiley-VCH, 2004).
13. Hopf, H. [22]Paracyclophanes in polymer chemistry and materials science. *Angew. Chem. Int. Ed.* **47**, 9808–9812 (2008).
14. Brown, C. J. & Farthing, A. C. Preparation and Structure of Di-*p*-Xylylene. *Nature* **164**, 915–916 (1949).
15. Cram, D. J. & Steinberg, H. Macro rings. I. Preparation and spectra of the paracyclophanes. *J. Am. Chem. Soc.* **73**, 5691–5704 (1951).
16. Cram, D. J. & Allinger, N. L. Macro rings. XII. Stereochemical consequences of steric compression in the smallest paracyclophane. *J Am Chem Soc* **77**, 6289–6294 (1955).
17. Rozenberg, V., Sergeeva, E. & Hopf, H. Cyclophanes as templates in stereoselective synthesis. In *Modern cyclophane chemistry* (eds Gleiter, R. & Hopf, H.) 435–462 (Weinheim, 2004).
18. Rowlands, G. J. The synthesis of enantiomerically pure [2.2]Paracyclophane derivatives. *Org. Biomol. Chem.* **6**, 1527–1534 (2008).
19. Gibson, S. E. & Knight, J. D. [2.2]Paracyclophane derivatives in asymmetric catalysis. *Org. Biomol. Chem.* **1**, 1256–1269 (2003).
20. Aly, A. A. & Brown, A. B. Asymmetric and fused heterocycles based on [2.2]Paracyclophane. *Tetrahedron* **65**, 8055–8089 (2009).
21. Paradies, J. [2.2]Paracyclophane derivatives: Synthesis and application in catalysis. *Synthesis* 3749–3766 (2011).
22. Delcourt, M.-L. *et al.* Highly enantioselective asymmetric transfer hydrogenation: A practical and scalable method to efficiently access planar chiral [2.2]Paracyclophanes. *J. Org. Chem.* **84**, 5369–5382 (2019).
23. Vorontsova, N. V. *et al.* Symmetrically tetrasubstituted [2.2]Paracyclophanes: Their systematization and regioselective synthesis of several types of Bis-bifunctional derivatives by double electrophilic substitution. *Chem. Eur. J.* **14**, 4600–4617 (2008).
24. David, O. R. P. Syntheses and applications of disubstituted [2.2]Paracyclophanes. *Tetrahedron* **68**, 8977–8993 (2012).
25. Hassan, Z., Spluling, E., Knoll, D. M., Lahann, J. & Bräse, S. Planar chiral [2.2]Paracyclophanes: From synthetic curiosity to applications in asymmetric synthesis and materials. *Chem. Soc. Rev.* **47**, 6947–6963 (2018).
26. Hassan, Z., Spuling, E., Knoll, D. M. & Bräse, S. Regioselective functionalization of [2.2]Paracyclophanes: Recent synthetic progress and perspectives. *Angew. Chem. Int. Ed.* **59**, 2156–2170 (2020).
27. Felder, S., Wu, S., Brom, J., Micouin, L. & Benedetti, E. Enantiopure planar chiral [2.2]Paracyclophanes: Synthesis and applications in asymmetric organocatalysis. *Chirality* **33**, 506–527 (2021).
28. Morisaki, Y., Hifumi, R., Lin, L., Inoshita, K. & Chujo, Y. Through-space conjugated polymers consisting of planar chiral pseudo-ortho-linked [2.2]Paracyclophane. *Polym. Chem.* **3**, 2727–2730 (2012).
29. Dekkers, H. P. J. M. Circularly polarized luminescence: A probe for chirality in the excited state. In *Circular Dichroism* 2nd edn (eds Berova, N. *et al.*) 185–215 (Toronto, 2000).
30. Riehl, J. P. & Richardson, F. S. Circularly polarized luminescence spectroscopy. *Chem. Rev.* **86**, 1–16 (1986).
31. Riehl, J. P. & Muller, F. *Comprehensive Chiroptical Spectroscopy* (Wiley and Sons, 2012).
32. Gon, M., Morisaki, Y., Sawada, R. & Chujo, Y. Synthesis of optically active X-shaped conjugated compounds and dendrimers based on planar chiral [2.2]Paracyclophane, leading to highly emissive circularly polarized luminescence. *Chem. Eur. J.* **22**, 2291–2298 (2016).
33. Maeda, H., Inoue, R., Saeki, A. & Morisaki, Y. Synthesis of optically active through-space conjugated polymers consisting of planar chiral pseudo-meta-disubstituted [2.2]Paracyclophane. *Polym. J.* **55**, 537–545 (2023).
34. Morisaki, Y., Gon, M., Sasamori, T., Tokitoh, N. & Chujo, Y. Planar chiral tetrasubstituted [2.2]Paracyclophane: Optical resolution and functionalization. *J. Am. Chem. Soc.* **136**, 3350–3353 (2014).
35. Miki, N., Inoue, R. & Morisaki, Y. Synthesis and chiroptical properties of one-handed helical oligo-o-phenylene-ethynylenes using planar chiral [2.2]Paracyclophane. *Bull. Chem. Soc. Jpn.* **95**, 110–115 (2022).
36. Namba, G., Mimura, Y., Imai, Y., Inoue, R. & Morisaki, Y. Control of axial chirality by planar chirality based on optically active [2.2]Paracyclophane. *Chem. Eur. J.* **26**, 14871–14877 (2020).
37. Sawada, R., Gon, M., Chujo, Y., Inoue, R. & Morisaki, Y. Synthesis of optically active π-stacked molecules: Effect of π-stacking position on the chiroptical properties. *Bull. Chem. Soc. Jpn.* **95**, 1353–1359 (2022).
38. Tsuchiya, M., Maeda, H., Inoue, R. & Morisaki, Y. Construction of helical structures with planar chiral [22]Paracyclophane: Fusing helical and planar chiralities. *Chem. Commun.* **57**, 9256–9259 (2021).
39. Oki, O. *et al.* Synchronous assembly of chiral skeletal single-crystalline microvessels. *Science* **377**, 673–678 (2022).
40. Roose, J., Tang, B. Z. & Wong, K. S. Circularly-polarized luminescence (CPL) from chiral AIE Molecules and macrostructures. *Small* **12**, 6495–6512 (2016).
41. Hu, M., Feng, H. T., Yuan, Y. X., Zheng, Y. S. & Tang, B. Z. Chiral AIEgens – Chiral recognition, CPL materials and other chiral applications. *Coord. Chem. Rev.* **416**, 213329 (2020).
42. Zhang, M. Y. *et al.* 2-(Dimesitylboryl)phenyl-substituted [2.2]Paracyclophanes featuring intense and sign-invertible circularly polarized luminescence. *Org. Lett.* **23**, 2–7 (2021).
43. Sawada, R., Gon, M., Nakamura, J., Morisaki, Y. & Chujo, Y. Synthesis of enantiopure planar chiral bis-(para)-pseudo-meta-type [2.2]Paracyclophanes. *Chirality* **30**, 1109–1114 (2018).
44. Sonogashira, K., Tohda, Y. & Hagihara, N. A convenient synthesis of acetylenes: Catalytic substitutions of acetylenic hydrogen with bromoalkenes, Iodoarenes and Bromopyridines. *Tetrahedron. Lett.* **16**, 4467–4470 (1975).
45. Sonogashira, K. Palladium-catalyzed alkynylation: sonogashira alkyne synthesis. In *Handbook of Organopalladium Chemistry for Organic Synthesis* (ed. Negishi, E.) 493–529 (New York, 2002).
46. Ogawa, K., Miki, N., Inoue, R. & Morisaki, Y. Correlation between orientation of the stacked π-electron systems and chiroptical properties. *ChemistrySelect* **8**, e202301844 (2023).
47. Sasai, Y., Tsuchida, H., Kakuta, T., Ogoshi, T. & Morisaki, Y. Synthesis of optically active π-stacked compounds based on planar chiral tetrasubstituted [2.2]Paracyclophane. *Mater. Chem. Front.* **2**, 791–795 (2018).
48. Xu, D. *et al.* The evident aggregation-induced emission and the reversible mechano-responsive behavior of carbazole-containing cruciform luminophore. *Dyes Pigm.* **172**, 107786 (2020).
49. Meng, L. *et al.* Twisted intramolecular charge transfer – Aggregation-induced emission fluorogen with polymer encapsulation-enhanced near-infrared emission for bioimaging. *CCC Chem.* **2**, 2084–2094 (2020).
50. Goldfinger, M. B., Crawford, K. B. & Swager, T. M. Directed electrophilic cyclizations: Efficient methodology for the synthesis of fused polycyclic aromatics. *J. Am. Chem. Soc.* **119**, 4579–4593 (1997).
51. Yang, J. *et al.* Boronate ester post-functionalization of PPEs: Versatile building blocks for Poly(2,2'-(1-(4-(1,2-di(thiophen-2-yl) vinyl)phenyl)-2-(2,5-dioctylphenyl)ethene-1,2-diyl)dithiophene) and application in field effect transistors. *J. Mater. Chem. C* **3**, 110074–110078 (2015).

Acknowledgements

The authors are grateful to Professor Kazuo Tanaka and Dr. Masayuki Gon (Graduate School of Engineering, Kyoto University) for CD and CPL spectroscopy. The financial support by Grant-in-Aid for Scientific Research (B) (No. 19H02792) from the Japan Society for the Promotion of Science is acknowledged (Y.M.). This work was also supported by the Murata Science Foundation (Y.M.).

Author contributions

K.J.: syntheses and structure determinations of all molecules in this manuscript, spectroscopic measurements (UV–vis, CD, PL, and CPL spectroscopies), writing – review and editing. R.I.: DFT and TD-DFT calculations, writing – review and editing. Y.M.: conceptualization and design of this study, supervision, project administration, funding acquisition, writing – original draft preparation.

Competing interests

The authors declare no competing interests.

Additional information

Supplementary Information The online version contains supplementary material available at https://doi.org/10.1038/s41598-023-49120-2.

Correspondence and requests for materials should be addressed to Y.M.

Reprints and permissions information is available at www.nature.com/reprints.

Publisher's note Springer Nature remains neutral with regard to jurisdictional claims in published maps and institutional affiliations.